NANO LETTERS

pubs.acs.org/NanoLett

Conductance Anisotropy in Epitaxial Graphene Sheets Generated by Substrate Interactions

Michael K. Yakes, Daniel Gunlycke, Joseph L. Tedesco, Paul M. Campbell, Rachael L. Myers-Ward, Charles R. Eddy, Jr., D. Kurt Gaskill, Paul E. Sheehan, and Arnaldo R. Laracuente*

U.S. Naval Research Laboratory, 4555 Overlook Avenue SW, Washington, D.C. 20375

ABSTRACT We present the first microscopic transport study of epitaxial graphene on SiC using an ultrahigh vacuum four-probe scanning tunneling microscope. Anisotropic conductivity is observed that is caused by the interaction between the graphene and the underlying substrate. These results can be explained by a model where charge buildup at the step edges leads to local scattering of charge carriers. This highlights the importance of considering substrate effects in proposed devices that utilize nanoscale patterning of graphene on electrically isolated substrates.

KEYWORDS Graphene, conductivity, four probe, SiC, anisotropy

Graphene has been a subject of intense research interest since the isolation of a single exfoliated sheet in 2004.[1] Being a sheet of carbon just one atom thick gives graphene many novel physical properties,[2,3] however, since it essentially has no "bulk" its entire volume is exposed to surface interactions.[4] Addressing these interactions will be crucial for graphene to fulfill its potential as a platform for many technological applications including digital electronics,[5] high frequency analog applications,[6,7] and spintronics.[8−10] For these applications, large area growth of high quality graphene films that are electrically isolated from their surroundings is required. Although many novel techniques for generating such films exist,[11,12] the most robust method to date for achieving this goal is graphene growth via thermal desorption of Si from SiC substrates. It is crucial to understand the influence of the substrate on the transport properties of the graphene. To this end, we present the first microscopic transport study of epitaxial graphene on SiC which demonstrates the effect of substrate steps on the electronic properties of the films.

The formation of epitaxial graphene on SiC by the thermal desorption of Si was first demonstrated in 2004 by Berger et al.[13] Recent advances in the field have produced graphene films as thin as a single atomic sheet that completely cover SiC wafers as large as 2 in. in diameter.[14,15] Epitaxial graphene on SiC has substantially different morphological and electrical properties dependent on which face of the SiC crystal the graphene is grown. Sheets grown on the C-face are typically multiple layers thick with each layer apparently rotationally decoupled from the others and therefore behaving as an isolated graphene sheet.[16] Morphologically, C-face samples have meandering steps and distinctive "giraffe stripes" that line the sample.[17,18] C-face samples show the highest electron mobilities with values greater than 18 000 $cm^2\ V^{-1}\ s^{-1}$ being reported at 300 K.[19] In contrast, Si-face samples have more uniform step bunches which are separated by ∼1 μm size terraces. Samples grown on the Si-face are often only one or a few layers thick and have lower mobilities (∼1000 $cm^2\ V^{-1}\ s^{-1}$) than their C-face counterparts.[15,19]

Because the SiC substrate is semi-insulating, the current device fabrication route envisions in situ lithography. Consequently, it is critical to determine the effect of the underlying substrate on the grown material.[20,21] To this end, thin graphene films were formed under high vacuum conditions on 4H-SiC(000$\bar{1}$) and 6H-SiC(0001) semi-insulating substrates with resistivity greater than 10^5 ohm-cm. After growth, the samples were characterized using Nomarski interference contrast microscopy, AFM, Raman spectroscopy, and Hall mobility measurements. Once a high quality wafer was found, it was loaded into a separate Omicron ultrahigh vacuum (UHV) Nanoprobe system containing a scanning electron microscope (SEM), scanning Auger microprobe, and four independent scanning tunneling microscopy (STM) tips for microscopic transport measurements. Use of the four-probe UHV STM was critical since it allowed placement of electrodes on specific terraces while eliminating potential sources of contamination that occur when electrodes are formed using conventional lift-off lithography.

To investigate the transport properties of the samples, we used the rotational square micro four-point probe method.[22,23] In this technique, the four probes are placed in a square configuration with 100 μm spacing between the probes as

* To whom correspondence should be addressed.
Received for review: 10/21/2009
Published on Web: 04/19/2010

DOI: 10.1021/nl9035302 | *Nano Lett.* **2010,** *10,* 1559–1562

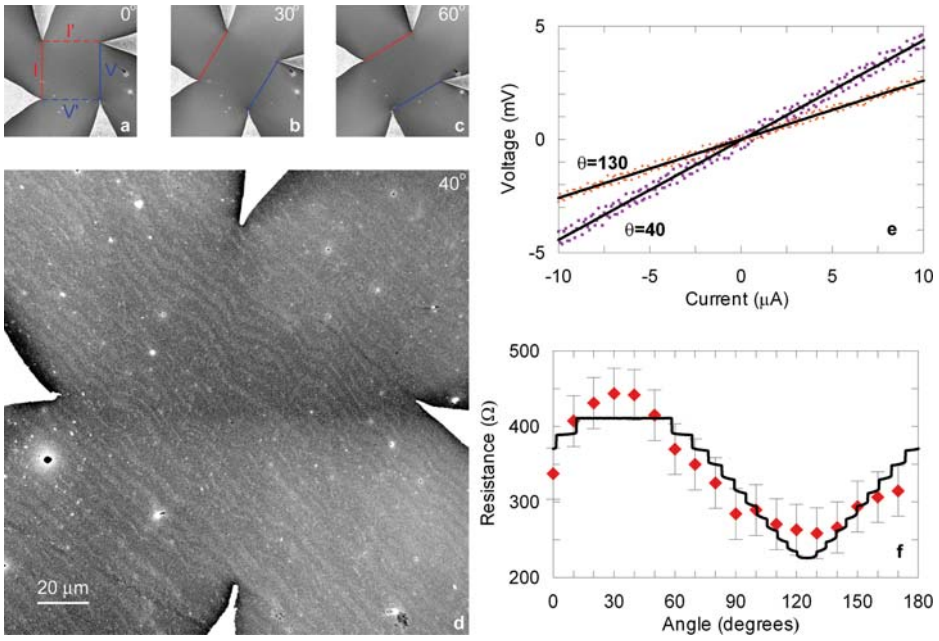

FIGURE 1. (a−c) Schematic diagram showing the rotational square micro four-probe technique at nominal angles 0, 30, and 60°, respectively. At each angle, current is passed through two adjoining tips while the voltage change is measured at the other set of two tips. By measuring two perpendicular configurations (e.g., I and I', V and V'), $V(I)$ curves at angles θ and $\theta + 90$ can be obtained. (d) A 40° tip configuration across the Si face sample. The direction of the step bunches can be identified with SEM (e) $V(I)$ curves for directions parallel ($\theta = 130$) and perpendicular ($\theta = 40$) to the step edges. The black lines are linear fits of the data through the origin. (f) Measured resistance vs angle. The fitted curve represents a model where scattering is increased at the step edges.

illustrated in Figures 1a−c. Current flowed from two adjoining tips in the square while the voltage difference is measured with the opposing two tips. Switching the tips that carry current and measure voltage allows quick measurement of transport in the perpendicular direction. Multiple rotations of the probes with respect to the substrate allow the conductivity to be mapped in all directions. Since the underlying SiC substrate was semi-insulating, we can neglect current flow through the substrate.

Figure 1d shows an SEM image of the four probes and graphene grown on a Si-face substrate with clearly defined parallel step bunches. These step bunches allow us to align the four probes parallel and perpendicular to the preferred step direction. Figure 1e shows voltage versus current plots taken parallel and perpendicular to the steps and shows a clear difference in the resistance depending on which direction the current flowed. The measured resistance parallel to the step edge is 260 Ω while the measured resistance perpendicular to the steps is 440 Ω. By measuring over a variety of angles, we mapped the resistance as a function of angle as shown in Figure 1f. The model that fits the data will be discussed shortly.

Since each probe can be moved independently we could confirm the anisotropic conduction with the slightly more cumbersome linear four probe measurements. We placed four probes in a line perpendicular to the step edges and all four probes on a single terrace as shown in Figure 2a,b. In each measurement, the spacing between the individual probes was 50 μm. These measurements were taken on a different area of the same sample used in Figure 1. The results of the voltage versus current curves taken in the two configurations are shown in Figure 2c, which confirms the strong dependence of the measured resistance on the direction of the probe spacing. The measured resistances are 660 Ω along the terrace and 940 Ω perpendicular to the steps. This compares to corresponding values of 320 and 560 Ω, respectively, for the square configuration at this location. The change in magnitude of the two measurements is expected due to different geometric prefactors in the two configurations.[22] Beyond confirming the result of the rotational square measurements, the linear four probe measurements reveal details about the nature of the conductance anisotropy. In an anisotropic thin film, different sources of anisotropy lead to different directional dependencies when measured by the linear four probe method. For an anisotropic material, the measured conductivity for four equally spaced probes in a linear configuration is independent of the orientation of the sample.[22] However, in an isotropic material where extrinsic effects such as step edges introduce anisotropy, the measured conductivity should be dependent on direction.[24] Since these experiments show a directional dependence the anisotropy is due to extrinsic effects. This is expected since the graphene dispersion of density of states is isotropic near the Fermi level.[25]

The C-face sample, while having a more complicated morphology, is the more promising candidate for technological applications due to its higher mobility. The changes in the morphology can be seen in the SEM images shown in

DOI: 10.1021/nl9035302 | *Nano Lett.* **2010,** *10,* 1559–1562

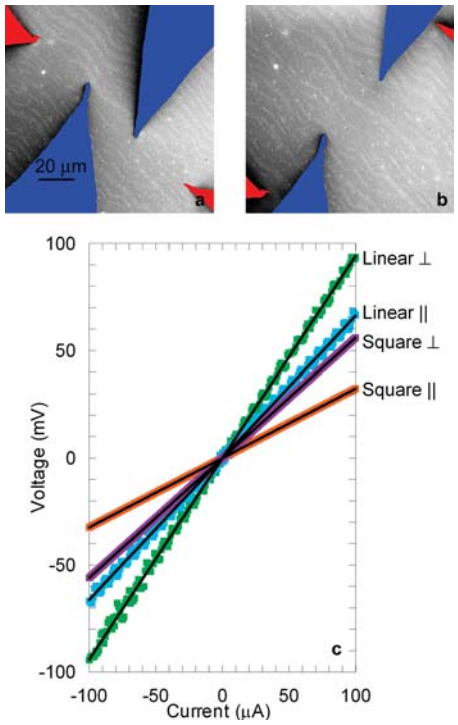

FIGURE 2. (a,b) SEM images showing the four probes aligned along a single terrace and perpendicular to the step edges. In the linear arrangement, constant current is passed through the outer two probes (colored red), while the voltage drop is measured between the inner two probes (colored blue). (c) *V*(*I*) curves measured along a single terrace and perpendicular to the steps with the linear and square four probe methods. Each method demonstrates higher resistance perpendicular to the step edges than parallel to the step edges.

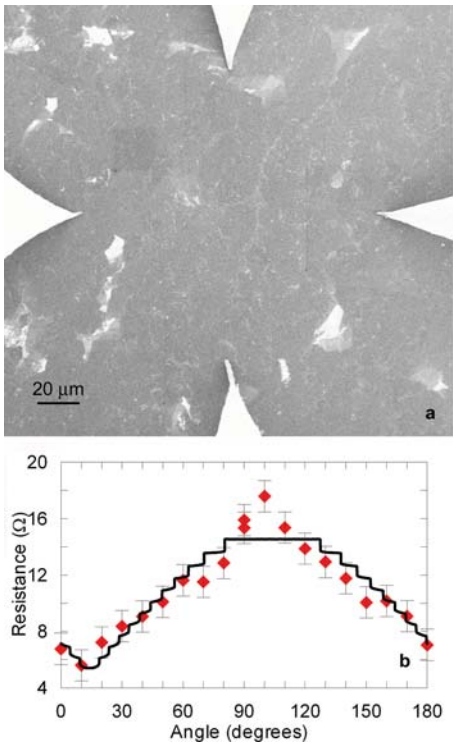

FIGURE 3. (a) SEM image showing morphology of the C-face sample with the four probes contacting the surface. Unlike the Si-face material, the direction of the graphene step edges is not observed in the SEM (b) Square four-probe resistance vs angle for the C-face sample. Anisotropy in conductance is observed in the material and is fit to the model where scattering is increased at the step edges.

Figure 3a. Instead of roughly parallel step bunches that line the sample there is instead a surface that appears rougher and individual steps cannot be resolved. Rotational square four probe measurements showed, as expected, that the C-face sample is more conductive that the Si-face sample. Surprisingly, the measurements also showed that conductivity varies as a function of angle. This was unexpected since the step edge morphology of the C-face is much less defined when compared to the Si-face sample and so from morphology alone one would not have intuitively predicted this noticeable anisotropy. This suggests that while AFM images show an erratic step edge structure on the graphene surface, the underlying interface retained some of its original step-terrace structure which influences the conductivity through the graphene.

The observed anisotropy could be explained through a phenomenological model. Because the scale of the nonuniformity is much greater than the mean free path, which ranges from a few nanometers up to hundreds of nanometers, the conductivity could be considered to be locally isotropic. The model assumes that there are 12 straight and evenly spaced step bunches within the distance $2a$, where $2a$ is the current-probe distance. If the step bunches are narrow compared to their separation, the current density paths are approximately those of infinitely thin step bunches. These paths are easily described using bipolar coordinates (η,ξ), where the current probes are located at $(\pm\infty,0)$. The conductivity for an arbitrary path is assumed to be of the form $\sigma(\xi) = [\rho_0/2 + N(\xi)R_0/L(\xi)]^{-1}$ for $|\xi| \leq \pi/2$ and 0 otherwise, where $N(\xi)$ is the number of crossed step bunches and $L(\xi) = 2a\xi/\sin\xi$ is the path length where ρ_0 is the resistivity of the material and R_0 is the resistance associated with crossing each step. By integrating over all the paths, the square four probe resistance R□ can finally be obtained. As can be seen in Figures 1f and 3b, the resistances given by this model agree qualitatively with the experimental data. The fitted parameters are $\rho_0 = 388\ \Omega$ and $R_0 = 42\ \Omega$ for the Si-face sample and $\rho_0 = 6.0\ \Omega$ and $R_0 = 1.9\ \Omega$ for the C-face sample.

Even though the quality of graphene grown on silicon carbide has improved rapidly,[15,19] it is believed that the dominant source of scattering remains silicon atoms trapped between neighboring graphene layers and between the lowest graphene layer and the substrate.[26] If the surface is terraced as in the present case, trapped silicon atoms are likely to aggregate at the step edges where they enhance scattering. Consequently, conduction anisotropy is a reflection of both geometric anisotropy and the extent of residual Si. For graphene grown on the C-face, the conductivity of the sample contains contributions from all layers and hence

DOI: 10.1021/nl9035302 | *Nano Lett.* **2010,** *10,* 1559–1562

Si-defects between different layers may also contribute to the scattering.

Other scattering mechanisms that have been shown to contribute to the resistivity in graphene were considered but discarded. Acoustic phonons in graphene have isotropic matrix elements, and therefore cannot contribute to the anisotropy.[27] Contributions from optical phonons are negligible for small bias voltages and would lead to nonlinear $V(I)$ characteristics, which were not observed.[28] Short-range scatterers and midgap states were found to be negligible for graphene on SiO_2.[29] The radius of curvature of the graphene over the steps is larger than or similar to the radius of carbon nanotubes where curvature-induced band gaps are at most of the order meV.[30,31] However, in order for curvature-induced gaps to lead to anisotropy, the graphene should have a carrier density of no more than 10^{10} cm^{-2}, which is much smaller than the measured carrier density in our experiments. Consequently, it is highly unlikely that curvature is responsible for the gap. Finally, though Raman spectroscopy measurements have shown that graphene is compressively strained across step features, the estimated 1 % change in lattice constant is not sufficient to induce the observed anisotropy.[32,33]

In summary, we show that the local conductivity of epitaxial graphene is dependent on the interaction between the graphene and the SiC substrate. We propose a model where charge buildup at the step edges lead to local scattering that influences the transport properties. This result highlights the importance of creating large uniform terraces in epitaxially grown graphene on SiC for future use in device applications. More generally, it suggests that no matter what method is used to generate the graphene a careful consideration of the underlying substrate will be required if optimal performance is to be achieved.

Acknowledgment. This work was supported by the Office of Naval Research and NRL's Nanoscience Institute. We thank Jim Culbertson for assistance with Raman spectroscopy measurements. M.K.Y. acknowledges support from the National Research Council Research Associate Program. J.L.T. acknowledges support from the American Society for Engineering Education Naval Research Laboratory Postdoctoral Fellowship program. D.G. thanks Carter T. White for discussions.

Supporting Information Available. Materials and methods. This material is available free of charge via the Internet at http://pubs.acs.org.

REFERENCES AND NOTES

(1) Novoselov, K. S.; Geim, A. K.; Morozov, S. V.; Jiang, D.; Zhang, Y.; Dubonos, S. V.; Grigorieva, I. V.; Firsov, A. A. *Science* **2004**, *306*, 666–669.
(2) Geim, A. K.; Novoselov, K. S. *Nat. Mater.* **2007**, *6*, 183–191.
(3) Geim, A. K. *Science* **2009**, *324*, 1530–1534.
(4) Schedin, F.; Geim, A. K.; Morozov, S. V.; Hill, E. W.; Blake, P.; Katsnelson, M. I.; Novoselov, K. S. *Nat. Mater.* **2007**, *6*, 652–655.
(5) Berger, C.; Song, Z.; Li, X.; Wu, X.; Brown, N.; Naud, C.; Mayou, D.; Li, T.; Hass, J.; Marchenkov, A. N.; Conrad, E. H.; First, P. N.; de Heer, W. A. *Science* **2006**, *312*, 1191–1195.
(6) Lin, Y.-M.; Jenkins, K. A.; Valdes-Garcia, A; Small, J. P.; Farmer, D. B.; Avouris, P. *Nano Lett.* **2009**, *9*, 422–426.
(7) Moon, J. S.; Curtis, D.; Hu, M.; Wong, D.; Campbell, P. M.; Jernigan, G.; Tedesco, J.; VanMil, B.; Myers-Ward, R.; Eddy, C., Jr.; Gaskill, D. K.; Robsinson, J.; Fanton, M.; Asbeck, P. *ECS Trans.* **2009**, *19*, 35–40.
(8) Tombros, N.; Jozsa, C.; Popinciuc, M.; Jonkman, H. T.; van Wees, B. J. *Nature* **2007**, *448*, 571–574.
(9) Son, Y.-W.; Cohen, M. L.; Louie, S. G. *Nature* **2006**, *444*, 347–349.
(10) Gunlycke, D.; Areshkin, D. A.; Li, J.; Mintmire, J. W.; White, C. T. *Nano Lett.* **2007**, *7*, 3608–3611.
(11) Sutter, P. W.; Flege, J.-I.; Sutter, E. A. *Nat. Mater.* **2008**, *7*, 406–411.
(12) Li, X.; Cai, X.; An, J.; Kim, S.; Nah, J.; Yang, D.; Piner, R.; Velamakanni, A.; Jung, I; Tutuc, E.; Banerjee, S. K.; Colombo, L.; Ruoff, R. S. *Science* **2009**, *324*, 1312–1314.
(13) Berger, C.; Song, Z.; Li, T.; Li, X.; Ogbazghi, A. Y.; Feng, R.; Dai, Z.; Marchenkov, A. N.; Conrad, E. H.; First, P. N.; de Heer, W. A. *J. Phys. Chem. B* **2004**, *108*, 19912–19916.
(14) Gaskill, D. K.; Jernigan, G. G.; Campbell, P. M.; Tedesco, J. L.; Culbertson, J. C.; VanMil, B. L.; Myers-Ward, R. L.; Eddy, C. R., Jr.; Moon, J.; Curtis, D.; Hu, M.; Wong, D.; McGuire, C.; Robinson, J. A.; Fanton, M. A.; Stitt, J. P.; Stitt, T.; Snyder, D.; Wang, X.; Frantz, E. *ECS Trans.* **2009**, *19*, 117–124.
(15) Emtsev, K. V.; Bostwick, A.; Horn, K.; Jobst, J.; Kellogg, G. L.; Ley, L.; McChesney, J. L.; Ohta, T.; Reshanov, S. A.; Rohrl, J.; Rotenberg, E.; Schmid, A. K.; Waldmann, D.; Weber, H. B.; Seyller, T. *Nat. Mater.* **2009**, *8*, 203–207.
(16) Hass, J.; Varchon, F.; Millan-Otoya, J. E.; Sprinkle, M.; Sharma, N.; de Heer, W. A.; Berger, C.; First, P. N.; Magnaud, L.; Conrad, E. H. *Phys. Rev. Lett.* **2008**, *100*, 125504.
(17) Biedermann, L. B.; Bolen, M. L.; Capano, M. A.; Zemlyanov, D.; Reifenberger, R. G. *Phys. Rev. B* **2009**, *79*, 125411.
(18) Luxmi;Fisher, P. J.; Srivastava, N.; Feenstra, R. M.; Sun, Y.; Kedzierski, J.; Healey, P.; Gu, G. *Appl. Phys. Lett.* **2009**, *95*, 073101.
(19) Tedesco, J. L.; VanMil, B.; Myers-Ward, R.; McCrate, J. M.; Kitt, S. A.; Campbell, P. M.; Jernigan, G. G.; Culbertson, J. C.; Eddy, C. R., Jr.; Gaskill, D. K. *Appl. Phys. Lett.* **2009**, *95*, 122102.
(20) Zhou, S. Y.; Gweon, G.-H.; Fedorov, A. V.; First, P. N.; de Heer, W. A.; Lee, D.-H.; Guinea, F.; Castro Neto, A. H.; Lanzara, A. *Nat. Mater.* **2007**, *6*, 770–775.
(21) Sutter, P. *Nat. Mater.* **2009**, *8*, 171.
(22) Kanagawa, T.; Hobara, R.; Matsuda, I.; Tanikawa, T.; Natori, A.; Hasegawa, S. *Phys. Rev. Lett.* **2003**, *91*, No. 036805.
(23) Matsuda, I.; Ueno, M.; Hirahara, T.; Hobara, R.; Morikawa, H.; Liu, C.; Hasegawa, S. *Phys. Rev. Lett.* **2004**, *93*, 236801.
(24) Wells, J. W.; Kallehauge, J. F.; Hoffman, Ph *Surf. Sci.* **2008**, *602*, 1742–1749.
(25) Wallace, P. R. *Phys. Rev.* **1947**, *71*, 622.
(26) Jernigan, G. G.; VanMil, B. L.; Tedesco, J. L.; Tischler, J. G.; Glaser, E. R.; Davidson III, A.; Campbell, P. M.; Gaskill, D. K. *Nano Lett.* **2009**, *9*, 2605–2609.
(27) Hwang, E. H.; Das Sarma, S. *Phys. Rev. B* **2008**, *77*, 11549.
(28) Yao, Z.; Kane, C. L.; Dekker, C. *Phys. Rev. Lett.* **2000**, *84*, 2941.
(29) Chen, J.-H.; Jang, C.; Ishigami, M.; Xiao, S; Cullen, W. G.; Williams, E. D.; Fuhrer, M. S. *Solid State Comm.* **2009**, *149*, 1080–1086.
(30) Coraux, J.; N'Diaye, A. T.; Busse, C.; Michely, T. *Nano Lett.* **2008**, *8*, 565–570.
(31) White, C. T.; Mintmire, J. W. *J. Phys. Chem. B* **2005**, *109*, 52–65.
(32) Robinson, J. R.; Wetherington, M.; Tedesco, J. L.; Campbell, P. M.; Weng, X.; Stitt, J.; Fanton, M. A.; Frantz, E.; Snyder, D.; VanMil, B. L.; Jernigan, G. G.; Myers-Ward, R. L.; Eddy, C. R., Jr; Gaskill, D. K. *Nano Lett.* **2009**, *9*, 2873–2876.
(33) Pereira, V. M.; Castro Neto, A. H.; Peres, N. M. R. *Phys. Rev. B* **2009**, *80*, No. 045401.

DOI: 10.1021/nl9035302 | *Nano Lett.* **2010,** *10,* 1559–1562